JOURNAL OF MATERIALS SCIENCE 24 (1989) 1670–1682

Notch sensitivity of thermoset and thermoplastic laminates loaded in tension

LEIF A. CARLSSON*, CARL-GUSTAF ARONSSON†, JAN BÄCKLUND†
*Department of Mechanical Engineering, Florida Atlantic University, Boca Raton, Florida 33431, USA
†Department of Aeronautical Structures and Materials, The Royal Institute of Technology, S-100 44 Stockholm, Sweden

Inplane tensile fracture of unnotched and notched thermoset graphite–epoxy and thermoplastic graphite–PEEK composite laminates is examined. Both fibre-dominated quasi-isotropic and matrix dominated ±45 angle-ply layups were investigated.

Classical lamination theory predictions of elastic and strength properties of unnotched specimens are compared with experiments. Several notched geometries, i.e. centre-notched, double-edge notched and open-hole specimens subjected to tensile loading to fracture were examined. The notched strength of the quasi-isotropic laminates was analysed by a damage zone model, where damage around the notch is represented by an "equivalent crack" with cohesive force acting between the crack surfaces.

Good agreement between experimental and calculated strength was observed for the graphite–epoxy laminates which failed in a collinear manner. For the graphite–PEEK laminates discrepancies between predicted and experimental strength are related to observed deviations from collinear crack growth. The angle-ply graphite–PEEK laminates showed larger notch sensitivity than the corresponding graphite–epoxy, probably due to less degree of stress relieving damage formation around the notch.

1. Introduction

Experimental data have shown that the tensile strength of composite laminates generally is severely reduced by the presence of a stress concentration in the form of a crack or a hole [1–8]. This appears to be related to the brittleness of the fibres used in advanced applications. Metals generally yield, making the presence of a stress concentration less severe. However, the strength of composite laminates is not reduced in inverse proportion to the stress concentration factor. This is explained by the opportunity that exists to reduce the local stress concentration by local damage creation mainly in the form of matrix micro-cracking and delamination. The type of damage and its growth is likely to depend on the state of stress in vicinity of the notch, the toughness of the matrix and the characteristics of the fibre–matrix interface.

In this context it is interesting to note that increased toughness of the matrix may or may not translate into a decreased notch sensitivity of the composite because of the material's lesser susceptibility to matrix cracking and delamination [9]. It is the purpose of this paper to investigate the notch sensitivity of two graphite fibre composites with matrices of widely different toughness, namely PEEK and epoxy. Both fibre-dominated quasi-isotropic layups and matrix-dominated ±45 angle-ply laminates will be investigated.

Commonly, strength of composite laminates in the presence of notches is analysed by the point stress criterion (PSC) [1, 2] or the inherent flaw model (IFM) [3]. The PSC and the IFM incorporate damage in an indirect manner, analogous to Irwin's plastic zone size correction [10] for homogeneous metals. More recently, however, a model has been proposed which takes the damage zone formation and growth more directly into account through the use of the finite element method [5–7]. This model, called the damage zone model (DZM), will be employed in the present work in order to analyse notched strength.

2. Damage zone model

The DZM was originally developed by Hillerborg *et al.* [11] for analysis of fracture of concrete and was later applied to fibrous composites by Bäcklund and Aronsson [5–7]. Only a brief description of the DZM will be presented here. A thorough description is given in references [5–7].

Consider a composite laminate plate with stress concentration, Fig. 1, subjected to an increasing external load, P. At a certain load level, damage in the form of matrix cracking and delamination will initiate in the highly stressed volume adjacent to the notch [12]. This is schematically shown in Fig. 2a. To simplify the modelling of the formation of damage, the damage zone is projected onto a straight line, an "equivalent crack", Fig. 2b, and treated by means of a Dugdale–Barenblatt type of analysis. Cohesive forces are assumed to act on the crack surfaces. With increased load an increase in the extent of damage in the material relates to an increase in crack opening, v, and reduced

0022–2461/89 $03.00 + .12

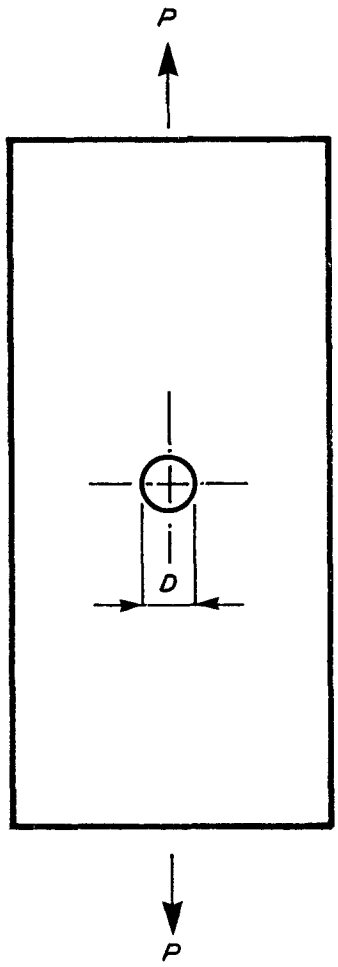

Figure 1 Composite laminate with a stress concentration subjected to an increasing load.

cohesive stress in the damage zone, see Fig. 3a. Assumption of a linearly decreasing cohesive stress with crack opening relationship, Fig. 3b, has given very good results for all laminated composites analysed to date [5–7]. The limiting stress, σ_0, Fig. 3b, is assumed to be equal to the unnotched tensile strength of the laminate. Note that in the modelling, only average orthotropic properties of the laminate are considered and the details on the ply level are neglected.

In the virgin unloaded material, there is no damage and hence no crack in the model. When the load is increased such that the maximum tensile stress at the notch reaches the unnotched tensile strength σ_0, the

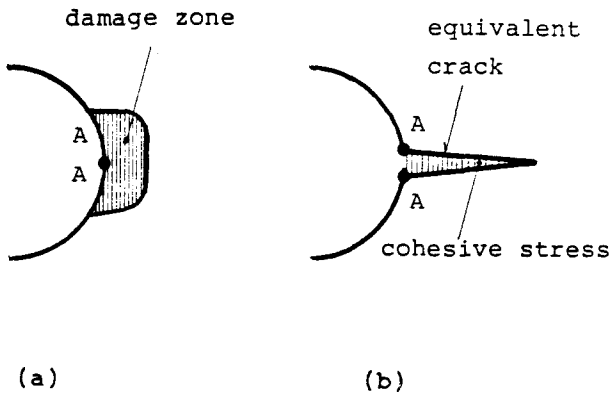

Figure 2 Damage zone at notch and equivalent crack used in analysis. (a) Damage zone and (b) equivalent crack.

equivalent crack is assumed to form. Upon further loading, this crack opens and grows into the composite thus representing increased damage. As a consequence of material softening due to damage formation, the cohesive stress along the crack is assumed to reduce as the crack opening increases, according to the linear relationship in Fig. 3b. Through this procedure, the nucleation and growth of damage, the associated redistribution of stress and stiffness change of the structure is modelled in a series of calculations using a condensed stiffness matrix computed by the finite element method (FEM). It should be pointed out that the area under the σ–v curve, Fig. 3b, represents the total fracture energy developed in the damage zone, and is denoted G_C^*. In the finite element modelling the material external to the damage zone is assumed to behave in a linear elastic manner. However, as a result of the softening in the damage zone the macroscopic stress–strain behaviour of the specimen may be non-linear.

3. Experimental details

3.1. Materials and specimens

Two composite materials were investigated in this study, namely a thermoset graphite–epoxy Hercules' (AS4/3501-6), and a thermoplastic graphite–PEEK ICI's (APC-2). It should be noted that both composites have AS4 fibres as the reinforcing phase. Laminates with stacking sequences $[0/90/\pm 45]_{2S}$ and $[\pm 45]_{4S}$ were manufactured at the Center for Composite Materials at University of Delaware. The thermoset material was processed in an autoclave

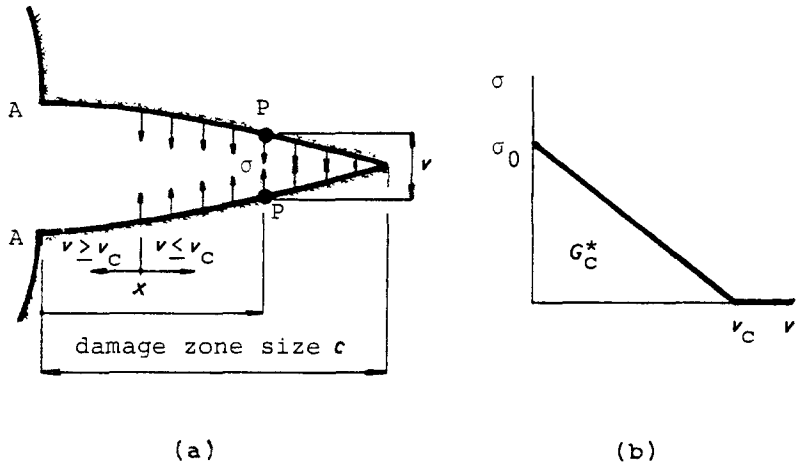

Figure 3 Dugdale–Barenblatt cohesive zone. (a) Crack with opening $v(x)$, cohesive stress $\sigma(x)$ and size c of the damage zone. (b) Assumed linear relation between σ and v.

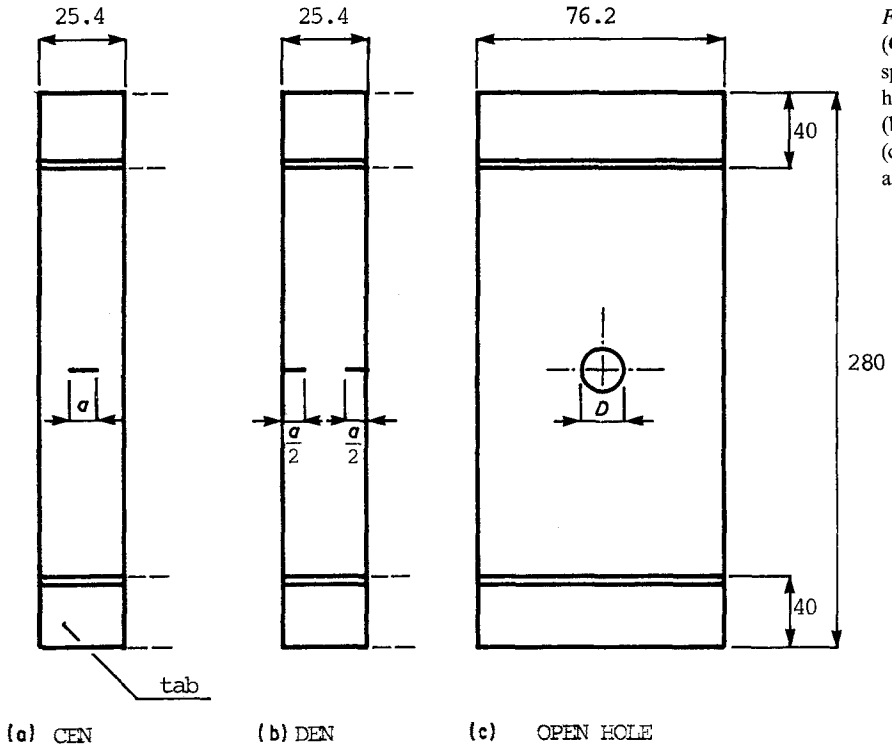

Figure 4 Dimensions for centre notched (CEN) and double-edge notched (DEN) specimens and specimens with circular holes. (a) CEN specimen, a = 6.35 mm, (b) DEN specimen, a = 12.7 mm and (c) open-hole specimen, D = 6.35, 12.7 and 25.4 mm.

according to the prepreg manufacturer's recommended cure cycle. The processing of the thermoplastic material was done in a Wabash Press according to a procedure that follows the prepreg manufacturer's recommendations. The rapid, post consolidation cooling required to attain the proper degree of crystallinity of the matrix, is achieved by cooling the press platens with an air–water mixture which provides an adequate cooling rate of about 40 °C min^{-1} over the critical temperature range of 380 to 200° C.

Tensile coupons, centre notched (CEN) and double-edge notched (DEN) specimens with geometries shown in Fig. 4 were machined from the plates. In order to obtain cracks in the CEN specimens, a 1 mm hole was drilled in the centre and a thin saw blade was inserted in the hole to create the crack. Cracks in the DEN specimens were machined with a solid carbide slitting saw* mounted in a horizontal milling machine. Finally, the tips of the cracks were sharpened with a razor blade. Open hole specimens, Fig. 4, with central holes of 6.35, 12.7 and 25.4 mm diameter, respectively, were also machined from the panels. Table I gives a summary of the dimensions and layups for all specimens investigated. At least five replicates of each geometry were made.

3.2. Mechanical testing

Tensile tests on unnotched tensile specimens instrumented and tested according to reference [13] were performed on an Instron testing machine using wedge action grips in order to determine Young's modulus, Poisson's ratio and the unnotched tensile strength, σ_0, of the laminates. All testing was performed at room temperature and ambient humidity conditions. The CEN, DEN and open hole specimen were tested in a standard tensile test frame at a crosshead rate of 1 mm min^{-1}.

4. Results and discussion

Table II gives experimentally determined tensile properties of the unnotched laminates as well as properties computed from classical lamination theory [14, 15]. All laminate strength calculations are based on the Tsai-Wu combined stress criterion [16] neglecting thermally and moisture induced residual stress. Strength values listed in Table II refer to last ply failure.

Lamina properties, Table III, required for this and subsequent analysis were obtained from previous investigations [17–19]. Good agreement between measured and predicted elastic properties is noted for

TABLE I Dimensions and layups for specimens investigated. L is the specimen length, w the specimen width, a the crack length and D the hole diameter. All dimensions are in mm

Specimen	Tensile	CEN	DEN	Open hole
Layup	$[0/90/\pm 45]_{2S}$	$[0/90/\pm 45]_{2S}$	$[0/90/\pm 45]_{2S}$	$[0/90/\pm 45]_{2S}$
Layup	$[\pm 45]_{4S}$	$[\pm 45]_{4S}$	-	$[\pm 45]_{4S}$
L	229	270	279	279
w	25.4	25.4	25.4	76.2
a	-	6.35	12.7	-
D	-	-	-	6.35, 12.7, 25.4

*Johansson Carbide Products Inc., Saginaw, Michigan, USA.

TABLE II Tensile properties of unnotched laminates. E_x is the axial Young's modulus, ν_{xy} Poisson's ratio and σ_x^{ult} the ultimate tensile strength ($=\sigma_0$)

Material	Layup	E_x (GPa)		ν_{xy}		σ_x^{ult} (MPa)	
		Experiment	Theory	Experiment	Theory	Experiment	Theory
AS4/3501-6	$[0/90/\pm45]_{2S}$	50.4	54.6	0.30	0.30	749 ± 50	668
AS4/3501-6	$[\pm45]_{4S}$	20.7	21.9	0.76	0.72	182 ± 11	153
APC-2	$[0/90/\pm45]_{2S}$	41.3	49.2	0.25	0.31	710 ± 25	826
APC-2	$[\pm45]_{4S}$	17.3	16.2	0.67	0.78	285 ± 25	262

both layups of the AS4/3501-6 material and the angle-ply APC-2 laminate, while the experimental Young's modulus and Poisson's ratio for the APC-2 quasi-isotropic laminate are lower than calculated. The difference may be due to fibre waviness present in APC-2 laminate. Fibre waviness introduced during processing of the laminates may possibly be due to buckling of the fibres in the matrix prior to solidification due to compressive residual thermal stresses induced in the 0° plies upon cool-down from the high processing temperatures of the AS4–PEEK material. Fibre waviness in AS4–PEEK laminates has recently been detected by O'Brien [20]. Agreement in ultimate strength is generally less favourable than for elastic properties depending on the inaccuracy of strength predictions and possible batch-to-batch variations.

4.1. Notched laminate strength

Notched strengths of CEN and DEN specimens are displayed in Table IV. The notched strength normalized with the unnotched strength (σ_N/σ_0) is also provided. It is observed that the quasi-isotropic layups are more sensitive to sharp notches than the angle-ply laminates, which tend to fail in a resolved shear mode rather than in net tension. Similar normalized notched strength values are observed for both material systems with quasi-isotropic layup. This may be expected since the response is dominated by the 0° fibres which are AS4 in both cases. The graphite–epoxy angle-ply laminates, on the other hand, retain a higher fraction (84%) of the unnotched strength than the corresponding graphite–PEEK laminates.

Table V gives open hole strengths for the two systems and layups. Also in this case both material systems with quasi-isotropic layup show similar notch sensitivity, the APC-2 system being slightly less notch sensitive (larger σ_N/σ_0) than the graphite–epoxy system. The angle-ply graphite–PEEK laminates, however, are substantially more notch sensitive than the angle-ply graphite–epoxy laminates, probably depending on the mode of fracture discussed in a subsequent section.

TABLE III Lamina properties for unidirectional AS4/3501-6 [18] and APC-2 [19]

	AS4/3501-6	APC-2
E_1 (GPa)	138	129
E_2 (GPa)	10.1	9.4
ν_{12}	0.29	0.31
G_{12} (GPa)	6.4	4.5
X_1^T (MPa)	1690	2140
X_1^C (MPa)	1450*	1254
X_2^T (MPa)	65	76
X_2^C (MPa)	146	214
S_6 (MPa)	81	141

*Data obtained from [19].

4.2. Fractography

Figs 5 and 6 show typical failure patterns of unnotched specimens and specimens with sharp notches. The CEN and DEN quasi-isotropic layups, Fig. 5 failed essentially in a net tension collinear crack propagation mode. The failure surfaces of the graphite–epoxy composites, Fig. 5a, showed higher extent of delamination than those of the graphite–PEEK material, Fig. 5b. The failure modes of the notched angle-ply graphite–epoxy laminates, Fig. 6, were similar to the mode of failure of the unnotched specimens, with matrix shear and delamination being the major features. The unnotched and notched graphite–PEEK angle-ply laminates, Fig. 6b, showed some fibre fractures besides matrix shear cracking and delamination. The less extensive matrix cracking and delamination of the fracture zone is probably due to the higher fracture toughness of the thermoplastic PEEK matrix [18].

Fig. 7 shows representative failure patterns of open-hole specimens. Since the mode of failure for each materials system and layup, judged by the appearance of the failed specimens, does not appear to depend on the hole size, only one hole size is shown. For the quasi-isotropic graphite–epoxy specimens, Fig. 7a, failure initiated on the hole boundary close to a horizontal axis through the centre of the hole and propagated across the width of the plate along the horizontal axis. Extensive delamination is evident between the ±45° angle-plies and matrix cracking occurred in these plies. Fig. 7b shows the failure pattern for the quasi-isotropic graphite–PEEK specimens. Different than in the graphite–epoxy specimen is that the failure propagated at 45° to the horizontal. This is evidently a result of the higher resistance to delamination of the graphite–PEEK system. If delamination is absent, crack propagation along the horizontal would require fibre fractures in both the +45° and −45° plies as well as in the 0° plies. Crack propagation at 45° to the horizontal requires fibre fractures in only half the angle-plies and hence constitutes a lower energy path. The graphite–epoxy angle-ply laminates, Fig. 7c, failed in a combination of inplane shear at 45° to the horizontal and delamination. Failure due to inplane shear appeared to initiate where the 45° fibres intersected the hole boundary, i.e. at 45° to the horizontal. However, broken fibres observed close to the hole boundary may indicate that a failure mechanism involving fibre fractures was operative in the initiation state. Fig. 7d

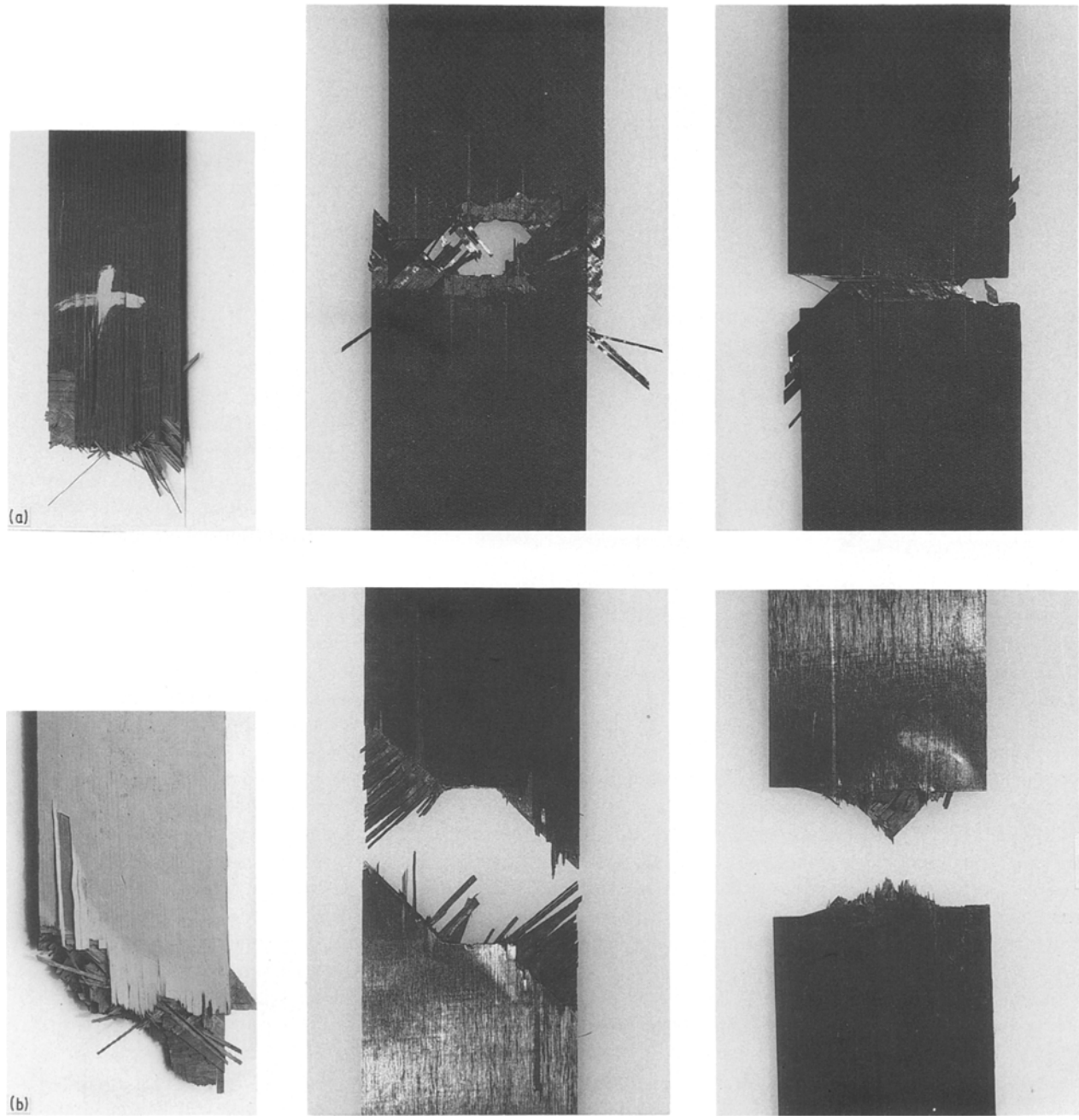

Figure 5 Failed unnotched and notched CEN and DEN quasi-isotropic laminates. (a) Graphite–epoxy and (b) graphite–PEEK.

shows that the graphite–PEEK angle-ply laminates with holes failed after large axial displacements resulting in extensive necking of the specimen and distortion of the initially circular hole. The failure mode was indicative to a lesser extent of delamination and larger extent of fiber fracture than the corresponding graphite-epoxy laminates, as a result of the tougher resin.

4.3. Correlation: DZM as opposed to experiment

In this section the damage zone model (DZM) is employed in order to analyse the experimentally obtained failure loads for specimens with quasi-isotropic layup. The strongly non-linear stress–strain behaviour of the ± 45 angle-ply specimens prohibited

TABLE IV Experimental notched strengths for CEN and DEN specimens. σ_N^{EXP} is the notched strength, σ_0 the unnotched strength, a the crack length and w the specimen width

Material	Layup	Test specimen	a/w	σ_N^{EXP} (MPa)	σ_N^{EXP}/σ_0
AS4/3501-6	$[0/90/\pm 45]_{2S}$	CEN	0.25	409 ± 23	0.546 ± 0.031
AS4/3501-6	$[0/90/\pm 45]_{2S}$	DEN	0.50	320 ± 11	0.427 ± 0.015
AS4/3501-6	$[\pm 45]_{4S}$	CEN	0.25	153 ± 8	0.841 ± 0.044
APC-2	$[0/90/\pm 45]_{2S}$	CEN	0.25	423 ± 6	0.596 ± 0.008
APC-2	$[0/90/\pm 45]_{2S}$	DEN	0.50	304 ± 14	0.428 ± 0.020
APC-2	$[\pm 45]_{4S}$	CEN	0.25	210 ± 6	0.737 ± 0.021

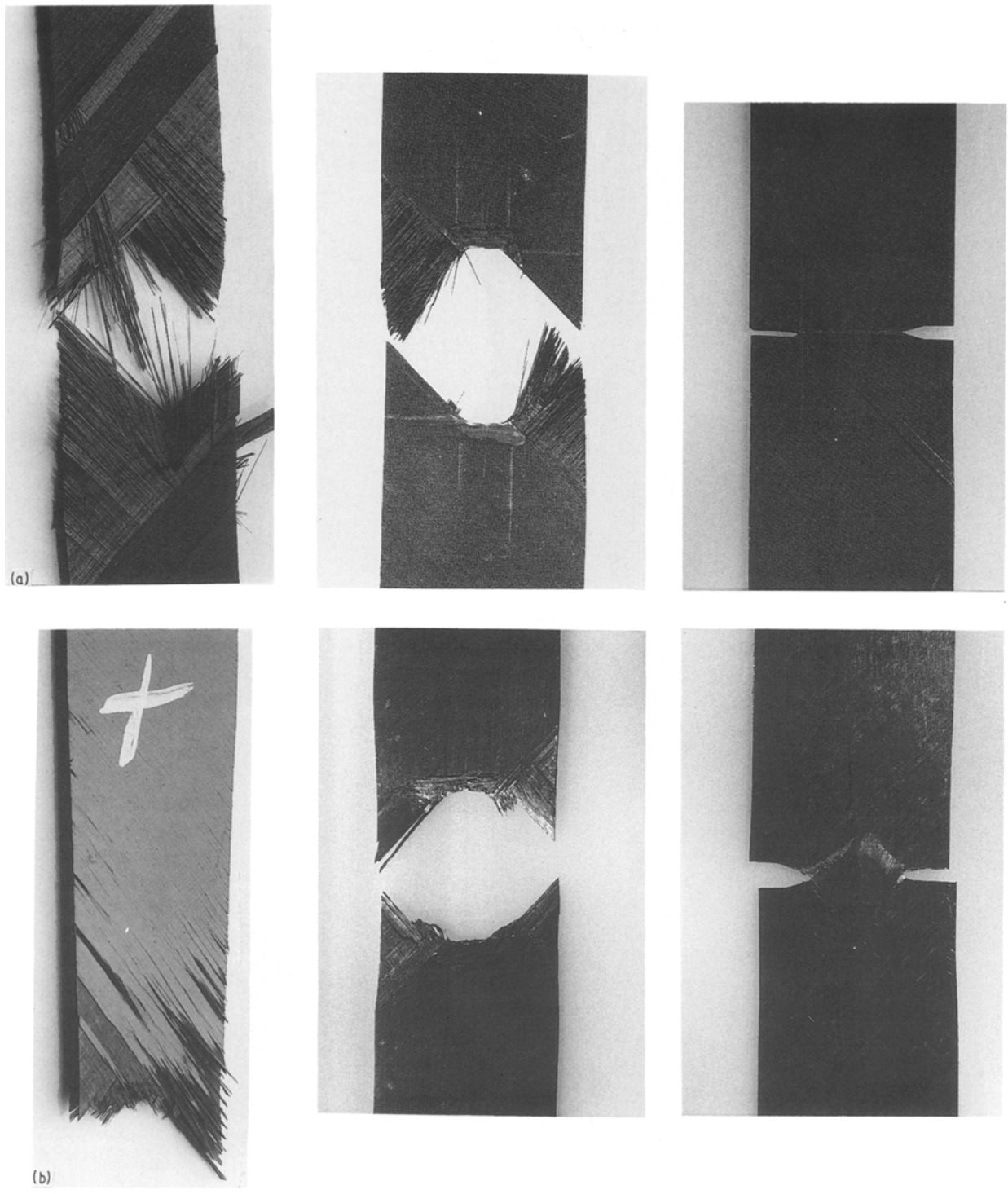

Figure 6 Failed unnotched and notched CEN and DEN ±45 angle-ply laminates. (a) Graphite–epoxy and (b) graphite–PEEK.

DZM calculations, based on linear elastic constitutive response to be performed.

To analyse notched strength a symmetry section of each specimen, shown in Fig. 4, was modelled by a suitable finite element (FE) mesh, and in all computations the general purpose finite element code GENFEM-3 developed by Glemberg *et al.* [21, 22] was used. A typical FE mesh, divided in four-node quadrilateral finite-elements with straight or curved sides, for one quarter of a specimen with circular hole is shown in Fig. 8. The length of the elements along the expected damage zone was 0.1 mm, Fig. 8b. The input data required for the DZM calculations are summarized in Table VI for the graphite–epoxy and graphite–PEEK laminates. To determine the apparent fracture energy, G_C^*, the average experimental fracture stress for the CEN specimens, Table IV, was used as a basis. For this purpose the strength (σ_N/σ_0) is calculated at given crack lengths for a series of G_C^* values by the DZM. Fig. 9 shows σ_N/σ_0 plotted against G_C^* for various crack lengths (a/w). Note that the curves in Fig. 9 are valid for both material systems considered. The appropriate value of G_C^* is the one giving agreement with the average experimental strength. In this manner $G_C^* = 65$ and 93 kJ m^{-2} were determined for the graphite–epoxy and graphite–PEEK quasi-isotropic specimens, respectively, see Fig. 9.

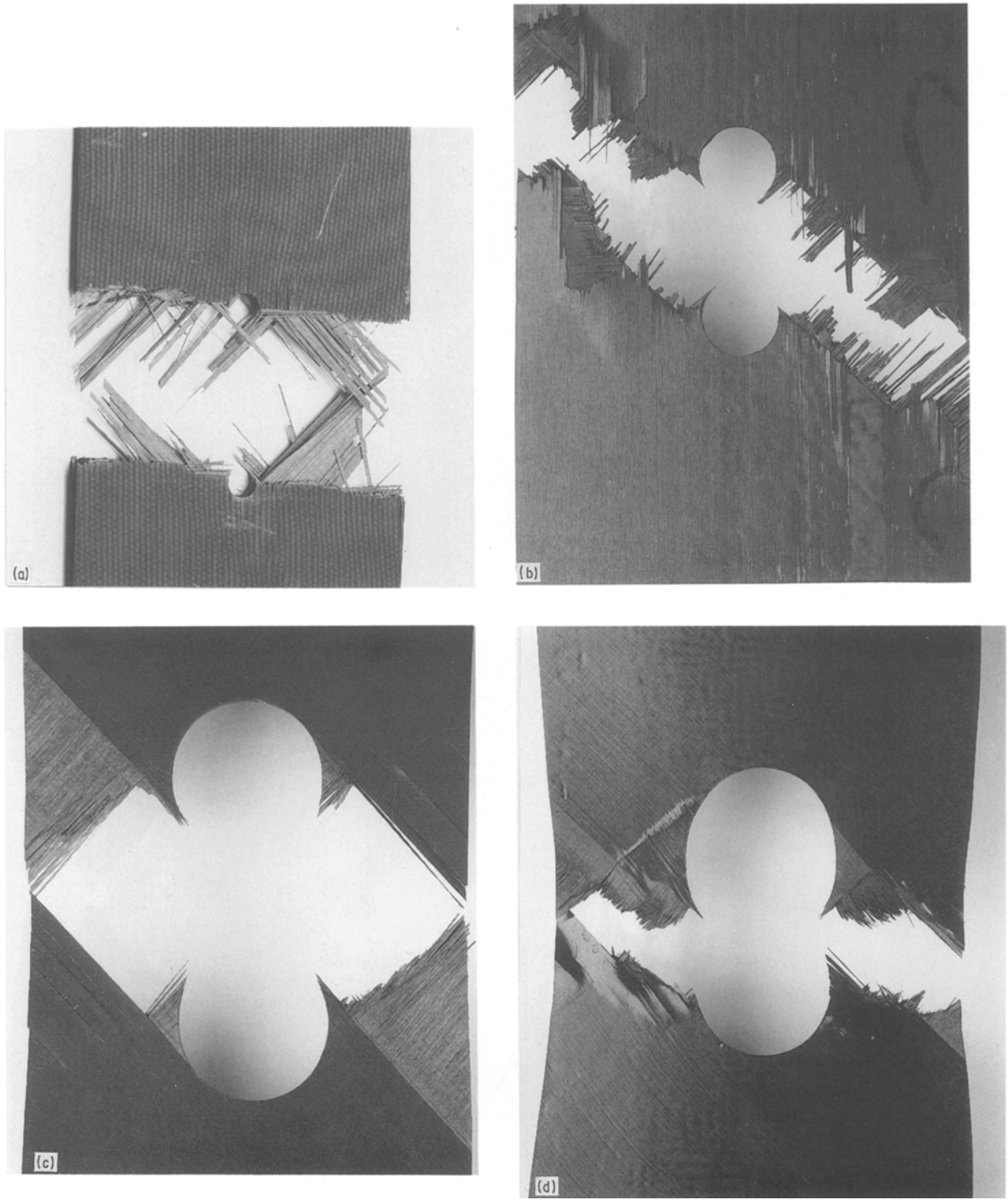

Figure 7 Failure patterns of open hole specimens. (a) $[0/90/\pm 45]_{2S}$ graphite–epoxy, (b) $[0/90/\pm 45]_{2S}$ graphite–PEEK, (c) $[\pm 45]_{4S}$ graphite–epoxy and (d) $[\pm 45]_{4S}$ graphite–PEEK.

Examination of the curves show that σ_N/σ_0 approaches zero as $G_C^* \rightarrow 0$ as they should. Furthermore, the slope of the curves increases with decreasing G_C^* and this is particularly pronounced for small values of a/w. This is further illustrated in Fig. 10 where σ_N/σ_0 is plotted against a/w for some G_C^* values around the value found for graphite–epoxy. Curves of σ_N/σ_0 plotted against G_C^* were determined in a similar manner for the quasi-isotropic DEN specimens, see Fig. 11. The curves are valid for the two material systems considered, and are similar in shape to the curves obtained for the CEN specimens in Fig. 9. In fact, a comparison between curves with the same width ratio in Fig. 9 and Fig. 11 show only a minor difference in predicted strength.

The G_C^* values determined from the CEN specimens can be used in subsequent strength predictions. Notched strength of the quasi-isotropic DEN specimens with $a/w = 0.5$, calculated from the DZM along with deviation from experiment is given in Table VII. Here, Δ^{DZM}, represents the percentage deviation between calculated and experimental strengths. The DZM underpredicts notched strength for both systems somewhat, especially for the graphite–epoxy system. This is probably due to a change in failure mode between specimen with a centre crack and edge crack,

TABLE V Experimental strength for specimens with circular holes. σ_N^{EXP} is the notched strength, σ_0 the unnotched strength, D the hole diameter and w the specimen width

Material	Layup	D (mm)	D/w	σ_N^{EXP} (MPa)	σ_N^{EXP}/σ_0
AS4/3501-6	$[0/90/\pm45]_{2S}$	6.35	0.083	420 ± 25	0.561 ± 0.033
AS4/3501-6	$[0/90/\pm45]_{2S}$	12.7	0.167	340 ± 13	0.454 ± 0.017
AS4/3501-6	$[0/90/\pm45]_{2S}$	25.4	0.33	262 ± 3	0.350 ± 0.004
AS4/3501-6	$[\pm45]_{4S}$	6.35	0.083	159 ± 7	0.868 ± 0.038
AS4/3501-6	$[\pm45]_{4S}$	12.7	0.167	153 ± 7	0.841 ± 0.038
AS4/3501-6	$[\pm45]_{4S}$	25.4	0.33	126 ± 2	0.692 ± 0.011
APC-2	$[0/90/\pm45]_{2S}$	6.35	0.083	385 ± 34	0.542 ± 0.048
APC-2	$[0/90/\pm45]_{2S}$	12.7	0.167	338 ± 13	0.476 ± 0.018
APC-2	$[0/90/\pm45]_{2S}$	25.4	0.33	260 ± 18	0.366 ± 0.025
APC-2	$[\pm45]_{4S}$	6.35	0.083	226 ± 11	0.793 ± 0.039
APC-2	$[\pm45]_{4S}$	12.7	0.167	181 ± 30	0.635 ± 0.105
APC-2	$[\pm45]_{4S}$	25.4	0.33	153 ± 24	0.537 ± 0.084

see Fig. 5. The specimens with an edge crack are less prone to delamination and show higher notched strength due to the larger extent of fibre fractures. Although the agreement may be considered satisfactory, this shows that the mode of failure is important and may change with crack geometry.

4.4. Open-hole specimens

Notched strength for the quasi-isotropic open-hole specimens was calculated from the DZM. All calculations are based on $G_C^* = 65$ and $93\,kJ\,m^{-2}$ determined previously from the CEN geometry for graphite–epoxy and graphite–PEEK, respectively.

Table VIII displays strength predictions for the quasi-isotropic specimens with circular holes. The agreement between the experimental and the predicted values is very good for the graphite–epoxy system. For graphite–PEEK, however, strength predictions for the smaller hole sizes are larger than the experimentally observed values. This is graphically illustrated in Figs 12 and 13 where notched strength predictions are plotted along with experimental values. The most obvious explanation to the deviation observed for the graphite–PEEK system is the lack of collinearity in crack growth, violating this assumption in the computations. Inspection of Fig. 7b shows that failure of the graphite–PEEK laminates propagated along the 45° direction, clearly violating the assumption of collinear crack growth in the strength modelling. Graphite–epoxy, on the other hand, Fig. 7a, shows collinear crack growth and good agreement between predicted and experimental strength, Fig. 12. Deviations from collinear crack growth could, in principle, be incorporated in the DZM. However, this involves mixed-mode crack propagation and constitutes a major complexity in the analysis. Altogether, considering the large variety in specimen geometry and failure modes the overall agreement between experiment and analysis lends confidence to the approach used. As a further illustration of the damage zone model, stress distribution curves along the assumed failure zone are shown in Fig. 14 at various load levels for a graphite–epoxy specimen with circular hole with $D/w = 0.167$. The stress σ_y normalized with σ_0 is plotted against the distance x ahead of the hole. For each stress distribution curve, denoted with a number,

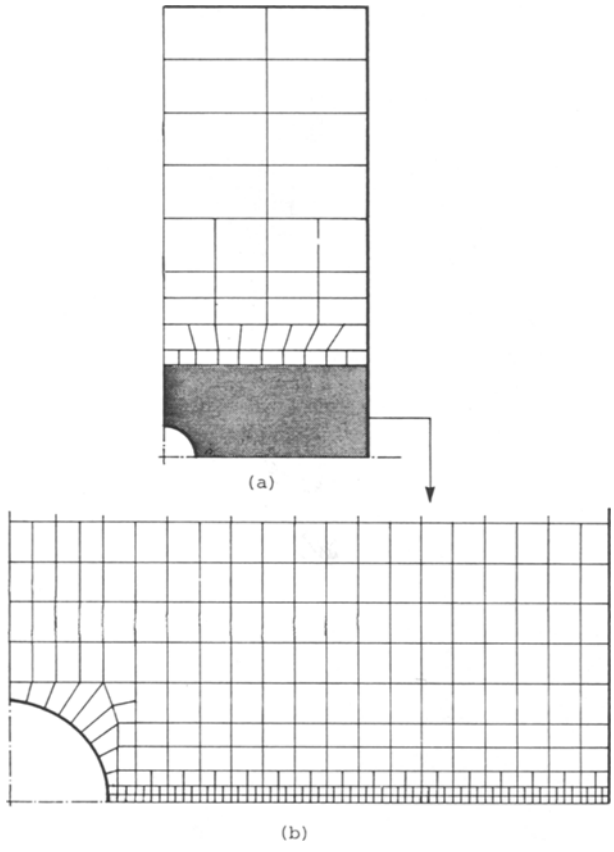

Figure 8 (a) Finite element mesh for one quarter of a specimen with circular hole and (b) refined part.

TABLE VI Input data used in the DZM calculations for quasi-isotropic AS4/3501-6 and the APC-2 laminates. Young's moduli, shear modulus and Poisson's ratio are calculated from ply data. σ_0 is the unnotched strength and G_C^* the apparent fracture energy

	AS4/3501-6	APC-2
E_x (GPa)	54.6	49.2
E_y (GPa)	54.6	49.2
ν_{xy}	0.30	0.31
G_{xy} (GPa)	21.2	18.9
σ_0 (MPa)	749	710
G_C^* ($kJ\,m^{-2}$)	65*	93*

*Based on CEN specimens with $a/w = 0.25$.

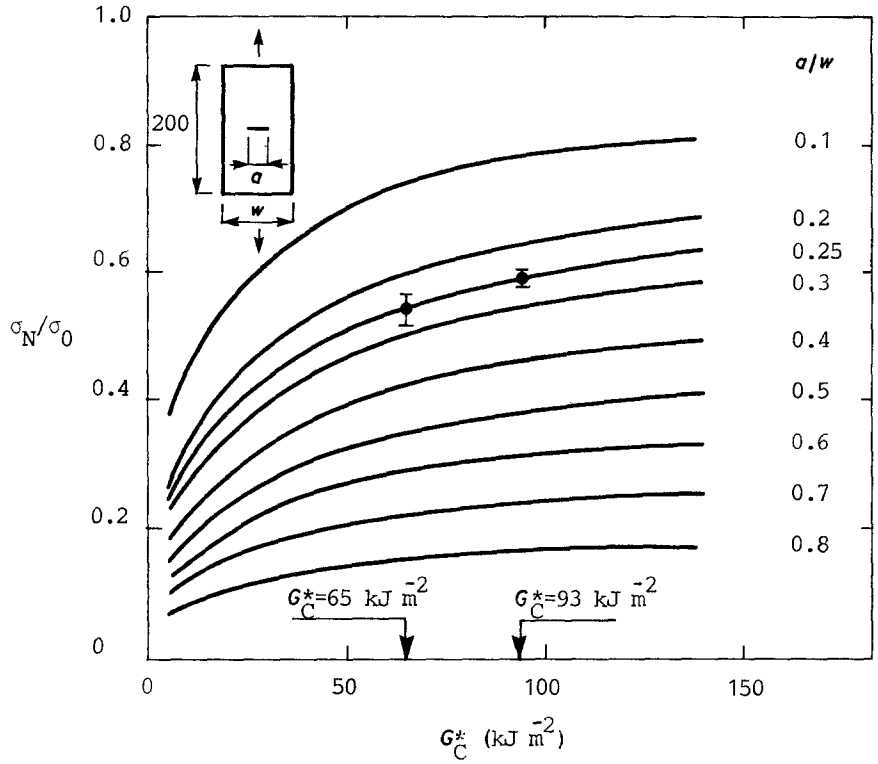

Figure 9 Notched strength (σ_N/σ_0) plotted against apparent fracture energy G_C^* for quasi-isotropic graphite–epoxy and graphite–PEEK CEN specimens (—— DZM, ♦ exp).

the damage zone extension is shown. When the external load is increased such that the stress at the second node away from the hole edge equals the unnotched strength σ_0, the equivalent crack is formed and the stress distribution curve denoted (1) is obtained, see Fig. 14. Upon further loading stable growth occurs until the critical damage zone size c_{crit} (curve (3)) is reached corresponding to a maximum in external load. Thereafter, unstable damage growth occurs and the external load decreases. It is noted that the stress σ_y in the damage zone decreases with the external load. c_{crit} was computed to be between 3.5 and 4.0 mm for all quasi-isotropic graphite–epoxy specimens. Corresponding values for the quasi-isotropic graphite–PEEK specimens are 5.0 to 5.75 mm, depending on the hole size. Note that in this modelling, the critical size of the damage zone is an *a priori* undetermined parameter. In the PSC and IFM a constant size of the damage zone is assumed [1, 3].

4.5. Open-hole angle-ply laminates

As mentioned previously, the strongly non-linear stress–strain response of the ±45 angle-ply laminates makes strength analysis based on linear elastic material behaviour less meaningful. Thus, in this section, only experimental results will be discussed.

Fig. 15 shows σ_N/σ_0 for graphite–epoxy and graphite–PEEK plotted against D/w along with a line based on strength reduction due to the reduced load carrying cross-sectional area

$$\frac{\sigma_N}{\sigma_0} = 1 - \frac{D}{w} \quad (1)$$

Equation 1 neglects any strength reduction due to the stress concentration at the hole boundary (which is only about 2 for ±45 laminates [13]). Inspection of Fig. 15 shows that the graphite–epoxy laminates conform very well to this line indicating virtually no influence of the stress concentration. The graphite–PEEK data, however, fall below the net section strength relation (Equation 1) indicating that the stress concentration due to the hole constitutes a strength reduction factor for this material. This may be explained by the lesser tendency of the PEEK

TABLE VII Predicted strength for quasi-isotropic DEN specimens. σ_N^{DZM} is the notched strength, σ_0 the unnotched strength, a the crack length and w the specimen width

Material	a/w	σ_N^{DZM} (MPa)	σ_N^{DZM}/σ_0	Δ^{DZM} (%)
AS4/3501-6	0.5	290	0.387	−9
APC-2	0.5	297	0.418	−2

where $\Delta^{DZM} = \left(\frac{\sigma_N^{DZM}}{\sigma_N^{EXP}} - 1\right) \cdot 100\%$

Input data
σ_0 = 749 MPa, G_C^* = 65 kJ m^{-2} for AS4/3501-6
σ_0 = 710 MPa, G_C^* = 93 kJ m^{-2} for APC-2

TABLE VIII Predicted strength for quasi-isotropic laminates with circular holes. σ_N^{DZM} is the notched strength, σ_0 the unnotched strength, D the hole diameter and w the specimen width

Material	D (mm)	D/w	σ_N^{DZM} (MPa)	σ_0^{DZM}/σ_0	Δ^{DZM} (%)
AS4/3501-6	6.35	0.083	440	0.587	+5
AS4/3501-6	12.7	0.167	344	0.459	+1
AS4/3501-6	25.4	0.33	262	0.350	±0
APC-2	6.35	0.083	461	0.649	+20
APC-2	12.7	0.167	366	0.515	+8
APC-2	25.4	0.33	266	0.375	+2

where $\Delta^{DZM} = \left(\frac{\sigma_N^{DZM}}{\sigma_N^{EXP}} - 1\right) \cdot 100\%$

Input data
σ_0 = 749 MPa, G_C^* = 65 kJ m^{-2} for AS4/3501-6
σ_0 = 710 MPa, G_C^* = 93 kJ m^{-2} for APC-2

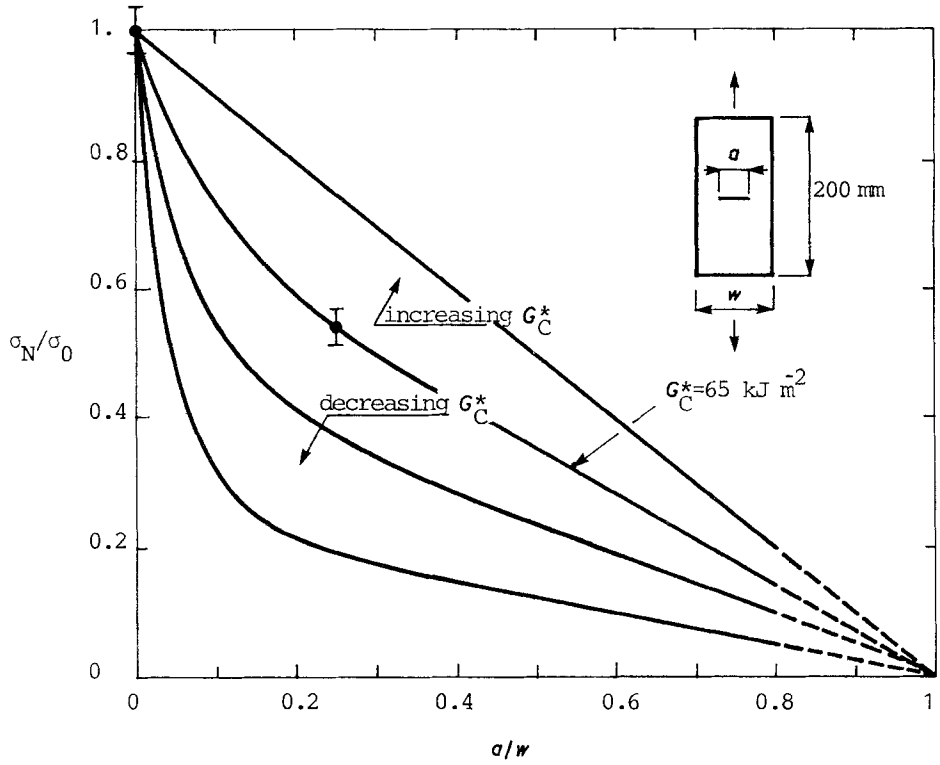

Figure 10 Notched strength (σ_N/σ_0) plotted against initial crack length (a/w) for quasi-isotropic CEN specimen (—— DZM, ♦ exp).

material to matrix cracking and delamination which relieve the localized stress concentration at the notch. Further support for this hypothesis is the CEN data in Table IV, where the graphite–PEEK angle-ply laminate shows significantly larger notch sensitivity than the corresponding graphite–epoxy layup.

5. Conclusions

Based on the results of this study, the following conclusions may be drawn; Classical lamination theory is generally a good predictor of elastic properties (Young's modulus and Poisson's ratio) for all laminates investigated. Fibre waviness introduced during the processing of the quasi-isotropic APC-2 material may, however, cause experimental stiffness and strength to fall below predicted values.

With regard to the behaviour of the notched laminates, the quasi-isotropic layups of both the materials showed similar notch sensitivity which might be expected due to the dominance of the load bearing zero degree fibres for these layups. For the ± 45 degree angle-ply laminates, however, significantly different notch sensitivity was observed between the materials due to the strong influence of the matrix

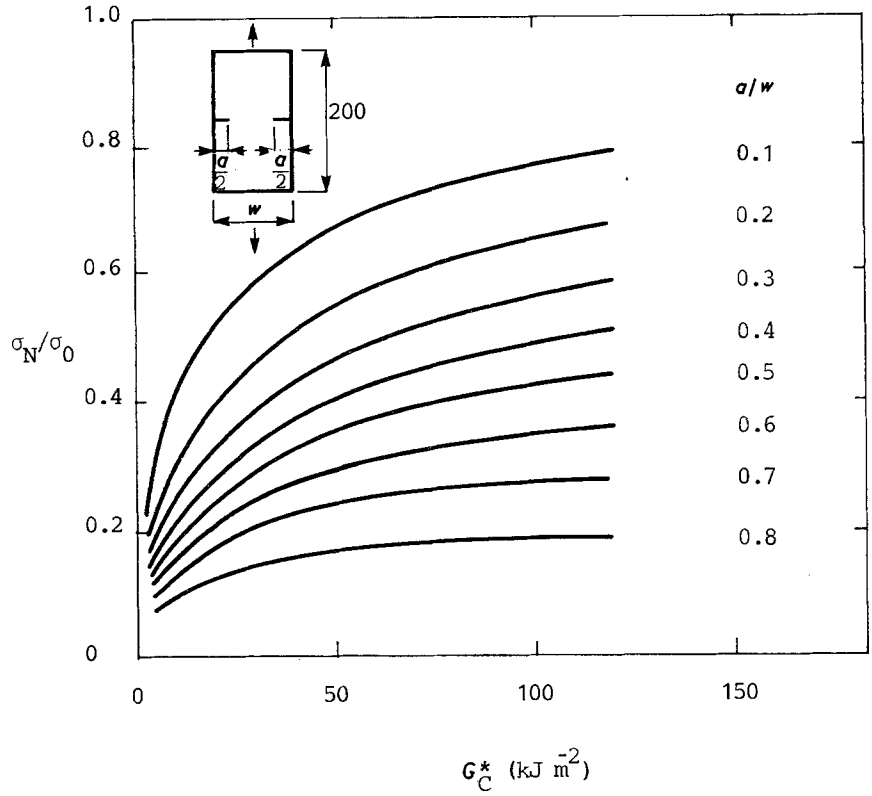

Figure 11 Notched strength (σ_N/σ_0) plotted against apparent fracture energy G_C^* for quasi-isotropic graphite–epoxy and graphite–PEEK DEN specimens (—— DZM, ♦ exp).

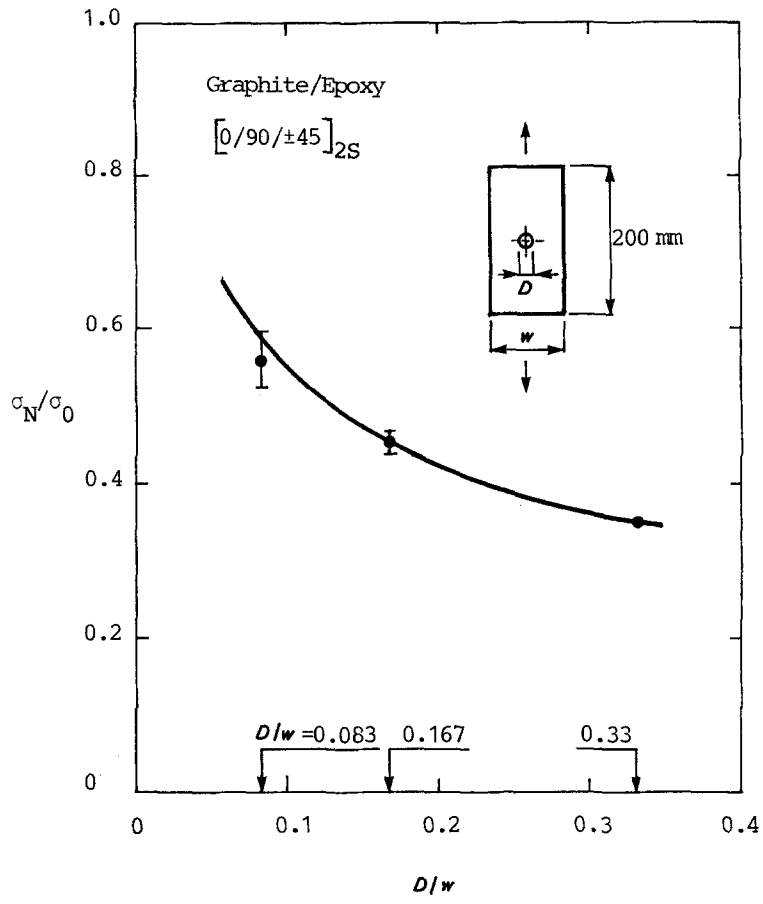

Figure 12 Notched strength (σ_N/σ_0) plotted against hole diameter (D/w) for graphite–epoxy specimens with circular holes (—— DZM, ⧫ exp).

shear response on the stress–strain response. The more brittle graphite–epoxy system exhibited very little influence of the presence of a stress concentration in the form of a crack or hole, probably depending on the local damage creation due to matrix cracking and delamination, which relieved the effect of the localized stress concentration.

The damage zone model (DZM) was employed to analyse strength of notched laminates. Only the quasi-isotropic layups were analysed because the strongly

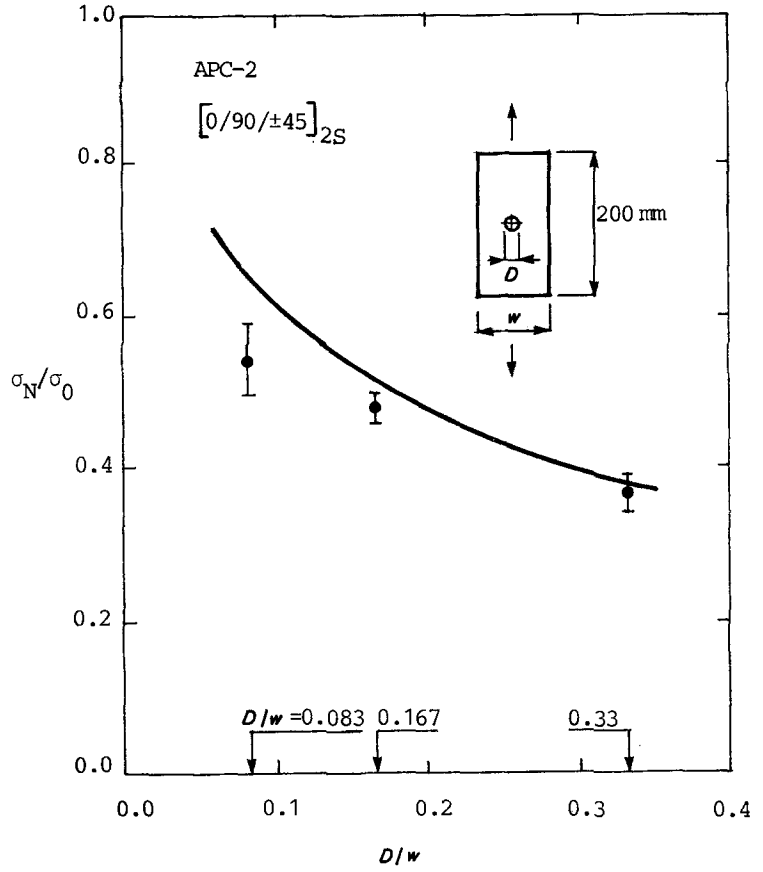

Figure 13 Notched strength (σ_N/σ_0) plotted against hole diameter (D/w) for graphite–PEEK specimens with circular holes (—— DZM, ⧫ exp).

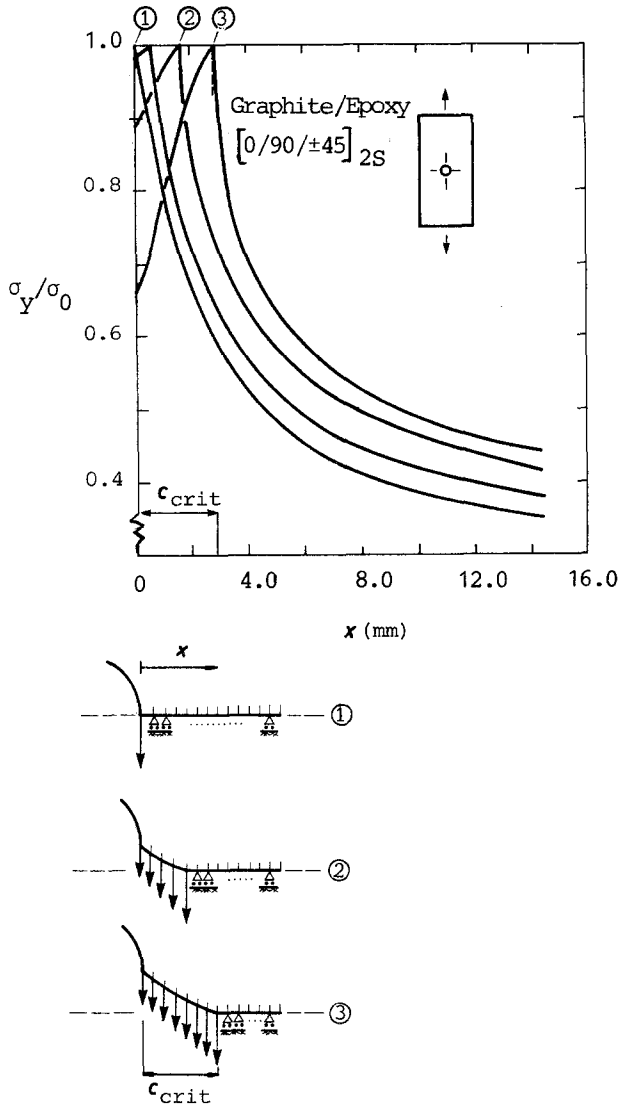

Figure 14 Normalized stress (σ_y/σ_0) plotted against x ahead of the circular hole at different external load levels for a specimen with circular hole.

non-linear stress–strain response of the angle-ply laminates rendered strength modelling based on linear elastic constitutive behaviour less meaningful. For the quasi-isotropic laminates the apparent fracture energy was determined from fracture tests of centre-notched specimens (CEN). Subsequent strength predictions for double-edge notched (DEN) and open-hole specimens were in overall good agreement with experimental values. However, the failure mechanism of the APC-2 laminates violated the assumption in the strength modelling of collinear crack growth resulting in measured strength being less than predicted. For the DEN graphite–epoxy specimens the predicted strength fell below measured values because of a larger extent of fibre fractures for this specimen. This shows that a constant failure mechanism is an important condition for a general application of the DZM. The computed size of the critical size of the damage zone was 3.5 to 4 mm and 5.0 to 5.8 mm for graphite–epoxy and graphite–PEEK quasi-isotropic laminates, respectively.

Acknowledgements

The experimental part of this study was performed at the Center for Composite Materials at the University of Delaware. The authors are grateful for assistance with processing, machining and testing the specimens by David C. Edwards and Tony Thirawong. Financial support for two of the authors (L. A. Carlsson and J. Bäcklund) from the Center/Industry consortium is gratefully acknowledged. Additional financial support from the Swedish Board for Technical Development (STU) under contract No. 85-2257, made it possible for one of the authors, C.-G. Aronsson, to contribute to this project.

References

1. J. M. WHITNEY and R. J. NUISMER, *J. Compos. Mater.* **8** (1974) 253.
2. R. J. NUISMER and J. M. WHITNEY, ASTM STP 593 (American Society for Testing and Materials, Philadelphia, 1975) p. 117.
3. M. E. WADDOUPS, J. R. EISENMANN and B. E. KAMINSKI, *J. Compos. Mater.* **5** (1971) 446.
4. R. B. PIPES, R. C. WETHERHOLD and J. W. GILLESPIE, *ibid.* **13** (1979) 148.
5. J. BÄCKLUND, *Comput. Struct.* **13** (1981) 145.
6. J. BÄCKLUND and C.-G. ARONSSON, *J. Compos. Mater.* **20** (1986) 259.

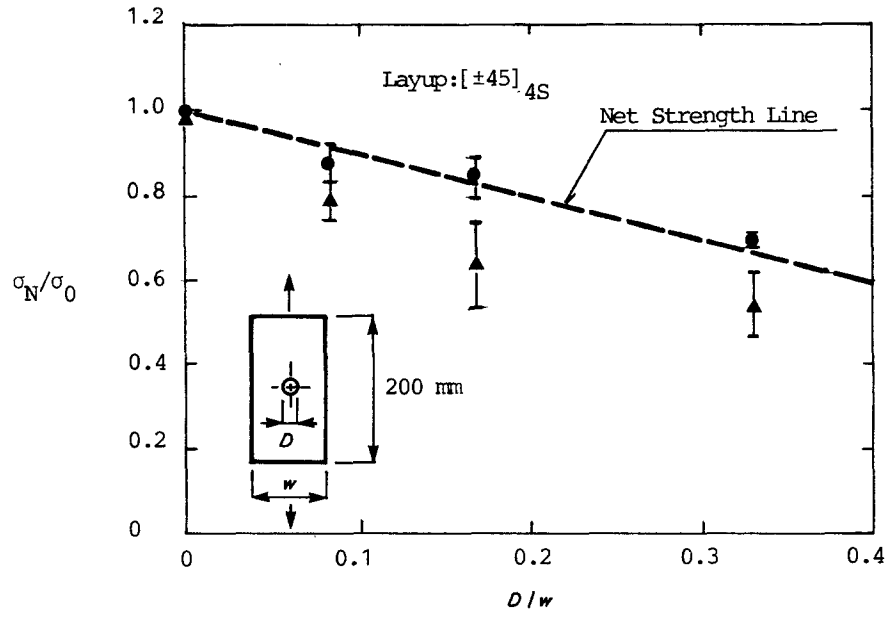

Figure 15 Notched strength (σ_N/σ_0) plotted against hole diameter (D/w) for graphite–epoxy (●) and graphite–PEEK (▲) ±45 angle-ply laminates.

7. C.-G. ARONSSON and J. BÄCKLUND, *ibid.* **20** (1986) 287.
8. J. AWERBUCH and M. S. MADHUKAR, *J. Reinf. Plast. Comp.* **4** (1985) 3.
9. S. M. BISHOP, G. D. HOWARD and C. J. WOOD, "The Notch Sensitivity and Impact Performance of (0, ±45) Carbon Fiber Reinforced PEEK", RAE Technical Report 84066 (HMSO, London, 1984).
10. F. A. MCCLINTOCK and G. R. IRWIN, ASTM STP 381 (American Society for Testing and Materials, Philadelphia, 1965) p. 84.
11. A. HILLERBORG, M. MODEER and P. E. PETERSON, *Cement Concrete Res.* **6** (1976) 773.
12. J. F. MANDELL, S. S. WANG and F. J. MCGARRY, *J. Compos. Mater.* **9** (1975) 266.
13. L. A. CARLSSON and R. B. PIPES, "Experimental Characterization of Advanced Composite Materials" (Prentice-Hall, New Jersey, 1987).
14. J. E. ASHTON, J. C. HALPIN and P. H. PETIT, "Primer on Composite Materials: Analysis" (Technomic, Westport, Connecticut, 1969).
15. "CMAP", Composite Software Users Guide, CCM, University of Delaware, Newark, DE (1984).
16. S. W. TSAI and E. M. WU, *J. Compos. Mater.* Vol. 5 (1971), p. 58.
17. R. WALSH, unpublished data, University of Delaware (1986).
18. J. W. GILLESPIE, Jr., L. A. CARLSSON, R. B. PIPES, R. ROTHSCHILDS, B. THRETHEWEY and A. SMILEY, "Delamination Growth in Composite Materials", NASA Contractor Report, NAG-1-475 (1985).
19. S. W. TSAI, "Composites Design – 1985" (Think Composites, Box 581, Dayton, Ohio, 1985).
20. T. K. O'BRIEN, "Fatigue Delamination Behavior of PEEK Thermoplastic Composite Laminates", Proceedings of the American Society for Composites First Conference on Composite Materials, Oct. 7–9 (1986), Dayton, OH.
21. H. WENNERSTRÖM, R. GLEMBERG and H. PETERSSON, "GENFEM-3, a computer program for general finite element analysis", User's Manual, Chalmers University of Technology, Department of Structural Mechanics, Publication 79:4, Göteborg, 1979.
22. H. WENNERSTRÖM and H. PETERSSON, "GENFEM-3, a computer program for general finite element analysis", Verification Manual, Chalmers University of Technology, Department of Structural Mechanics, Publication 79:5, Göteborg, 1979.

Received 9 May
and accepted 12 September 1988